Role of the Atmospheric and Oceanic Circulation in the Tropical Pacific SST Changes

JINGZHI SU

Nansen-Zhu International Research Centre, Institute of Atmospheric Physics, Chinese Academy of Sciences, Beijing, China, and Nansen Environmental and Remote Sensing Center, Bergen, Norway

HUIJUN WANG

Nansen-Zhu International Research Centre, Institute of Atmospheric Physics, Chinese Academy of Sciences, Beijing, China

HAIJUN YANG

Department of Atmospheric Science, School of Physics, Peking University, Beijing, China

HELGE DRANGE, YONGQI GAO, AND MATS BENTSEN

Nansen-Zhu International Research Centre, Institute of Atmospheric Physics, Chinese Academy of Sciences, Beijing, China, and Nansen Environmental and Remote Sensing Center, and Bjerknes Centre for Climate Research, Bergen, Norway

(Manuscript received 25 September 2006, in final form 13 September 2007)

ABSTRACT

A coupled climate model is used to explore the response of the tropical sea surface temperature (SST) to positive SST anomalies in the global extratropics. The main model results here are consistent with previous numerical studies. In response to prescribed SST anomalies in the extratropics, the tropical SSTs rise rapidly and reach a quasi-equilibrium state within several years, and the tropical subsurface temperatures show a slow response. The annual-mean Hadley cell, as well as the surface trades, are weakened. The weakened trades reduce the poleward Ekman transports in the tropical ocean and, furthermore, lead to anomalous positive convergences of heat transport, which is the main mechanism for maintaining the tropical Pacific SST warming.

The process of an extratropical influence on the tropics is related to both the atmospheric and oceanic circulations. The intertropical convergence zone (ITCZ) moves southward and eastward in the Pacific, corresponding to a reduction of the Hadley circulation and Walker circulation. At the same time, convective precipitation anomalies are formed on the boundary of the climatological ITCZ, while the climatological mean convections centered in the Southeast Asia region are suppressed. The largely delayed response of the tropical subsurface temperature cannot be explained only by the strength change of the subtropical cells (STCs), but can be traced back to the slow changing of subsurface temperature in the extratropics. In the extratropical oceans, warming and freshening reduce the surface water density, and the outcropping lines of certain isopycnal layers are moved poleward. This poleward movement of outcropping lines can weaken the positive temperature anomalies, or even lead to negative anomalies, on given isopycnal layers. Displayed on time-dependent isopycnal layers, positive subsurface temperature anomalies are present only in the region after subduction, and are subsequently replaced by negative temperature anomalies in the deep tropics regions. The noticeable features of the density compensation of temperature and salinity indicate that diapycnal processes play an important role in the equatorward transport of the temperature and salinity anomalies from the midlatitude.

1. Introduction

The tropics are a key region in the global climate system because of the strong solar heating and the pronounced climate fluctuations on interannual to interdecadal time scales; the area has important, far-reaching climatic and socioeconomic impacts on local and remote regions (e.g., Lau 1997; Alexander et al. 2002). For example, the tropical climate and its variations can influence the North Pacific (Zhang and Wallace 1996), the North Atlantic (Hoerling et al. 2001; Lu et al. 2004), and the climate of North America (e.g., Barlow et al. 2001).

Corresponding author address: Dr. Jingzhi Su, Nansen-Zhu International Research Centre, IAP/CAS, ChaoYang District, Beijing 100029, China.
E-mail: sujz@mail.iap.ac.cn

DOI: 10.1175/2007JCLI1692.1

Theories have been proposed to explain the mechanisms for the tropical climate variability and the associated teleconnection patterns. In addition to the local sources of the dynamic processes in the tropical ocean–atmosphere system (e.g., Knutson and Manabe 1998; Kirtman and Schopf 1998), the climate fluctuations in the extratropics may also lead to changes in the tropical climate through atmospheric and oceanic teleconnections [hereafter the atmospheric bridge and ocean tunnel; see a review by Liu and Alexander (2007)]. It is shown that the strongest decadal SST and ocean heat content anomalies occur at midlatitudes (Giese and Carton 1999). The decadal midlatitude changes over the North Pacific can cause decadal modulation of El Niño–Southern Oscillation (ENSO) through an atmospheric bridge (e.g., Barnett et al. 1999). Subtropical SST anomalies in winter may persist into spring and summer, and may induce a broad-scale atmospheric response influencing the tropics (Vimont et al. 2003). Oceanic teleconnection signals are also involved in the extratropics-forced low-frequency variability of the tropics by means of changes in the shallow subtropical overturning circulation (Kleeman et al. 1999), or by anomalies in the temperature of the upwelled equatorial waters (Gu and Philander 1997). The latter can be caused by an anomalous deep thermocline or by changes in the temperature on the isopycnals (Schneider 2000; Giese et al. 2002).

Although the extratropical SST variabilities are associated with several dominant modes (e.g., Pacific decadal oscillation; North Atlantic/Arctic Oscillation, NAO/AO) and they may exert different influences on the tropical climate, the conception of teleconnection including zonal-mean extratropical and tropical anomalies is essentially useful. This generalization of teleconnection patterns allows us to think about the climate variability of various spatial and temporal scales in a more unified framework (Liu and Alexander 2007). More recently, using a so-called partial coupling technique in a fully coupled climate model, Yang and Liu (2005, hereafter YL05) and Liu and Yang (2003) performed numerical sensitivity tests with SST anomalies of 2°C in the global extratropics and identified that the extratropical impact on the tropics could be as strong as the tropical impact on the extratropical climate. However, there are still several questions remaining to be clarified. For instance, the possibility that such results are model dependent has not been excluded. The resolution (1.4° latitude × 2.8° longitude) of the ocean model in YL05 is somewhat rough relative to the complex tropical ocean current system. The evolutions of anomalous signals on isopycnals, which play a central role in the ocean tunnel, need to be described.

In this study, numerical experiments are designed following YL05 with the aim of exploring the key processes governing the tropical SST anomalies under the forcing of the extratropical prescribed SST anomalies. The mechanisms responsible for maintaining anomalous tropical SSTs are in focus. Special attention is paid to the role of the annual-mean atmospheric meridional circulation (the Hadley cells) and the shallow oceanic meridional circulation [the subtropical cells, (STCs)], the latter with particular focus on the Pacific Ocean. Studies of the climate effects of the prescribed SST anomalies in certain region can be understood as being relevant to the problem of mechanisms of climate adjustment to slow external forcing. We expect that the physical processes examined here and our understanding of climate adjustment to external forcing could be helpful in understanding reality in the study of global climate changes.

The paper is arranged as follows. Section 2 introduces the coupled model and sensitivity experiments performed. Section 3 examines the simulated extratropical impact on the tropical climate. In section 4, an analysis of the heat budget is provided, including quantification of the zero-, first-, and second-order terms of the heat advection. Section 5 investigates the mechanisms concerning the changes in the Hadley cells, the STCs, and the subsurface temperature. Discussion and conclusions are given in section 6.

2. Model description and setup of the experiment

The coupled atmosphere–ocean model used in this study is the Bergen Climate Model (BCM; Furevik et al. 2003; Bentsen et al. 2004; Sorteberg et al. 2005), consisting of the atmospheric Action de Recherche Petite Echelle Grand Echelle/Integrated Forecast System (ARPEGE/IFS; Déqué et al. 1994) general circulation model (GCM) and the Miami Isopycnic Coordinate Oceanic Model (MICOM; Bleck et al. 1992). The latter is fully coupled with a dynamic and thermodynamic sea ice model (Drange and Simonsen 1996).

ARPEGE/IFS is run on a linear T_L63 grid (horizontal resolution is about 2.8° × 2.8°) with 31 vertical levels, ranging from the surface to 0.01 hPa. MICOM is configured with a horizontal Mercator grid mesh with one pole over Siberia and the other over Antarctica, and with a nominal resolution of about 2.4° × 2.4°. The horizontal resolution in MICOM is increased to 0.8° in a band along the equator to better resolve equatorial dynamics. MICOM has 24 layers in the vertical, including an uppermost mixed layer, with temporal and spatial varying density, and 23 isopycnal layers below with prescribed potential densities ranging from $\sigma_0 = 24.12$

to $\sigma_0 = 28.10$. The sea ice model is on the same horizontal grid as MICOM. It is noted that the model resolution in this study is similar to (or somewhat higher than) that in YL05, which has an atmospheric resolution of R15 with 18 vertical layers in a hybrid sigma-pressure coordinate system and an oceanic resolution of 1.4° latitude × 2.8° longitude × 32 vertical levels.

For the model's setup and spinup details, please refer to Furevik et al. (2003) and Bentsen et al. (2004). A 300-yr control integration (BCM_{CTRL}), presented in Furevik et al. (2003), forms the basis for the perturbation experiments presented here. The BCM can capture the main present climate features. For instance, the strength and position of the simulated Hadley cells are close to those of the National Centers for Environmental Prediction's (NCEP's) estimates. The maximum value and structure of the simulated Atlantic Ocean meridional overturning circulation are consistent with previous results (Furevik et al. 2003). The two strongest natural modes of variability in the global climate, the ENSO and the NAO/AO, were captured by the BCM (Furevik et al. 2003; Zhou et al. 2006a,b).

To quantify the impact of the extratropics on the tropics, a so-called atmospheric bridge–ocean tunnel (ABOT; Liu and Yang 2003; YL05) experiment is performed. The ocean and atmosphere in the ABOT remain fully coupled within the global tropics, here defined as being equatorward of 25°. In the extratropical world oceans (i.e., poleward of 35° but excluding the seasonal maximum sea ice extent regions in the Arctic and Antarctic), a 2°C SST anomaly is "seen" by both the atmosphere and ocean by means of partial coupling (Wu et al. 2003, YL05). In the partially coupled region, the atmosphere is forced with a heat flux that is calculated based on prescribed monthly climatological SSTs from BCM_{CTRL} plus a 2°C SST anomaly, while the heat flux, freshwater, and momentum that drive the ocean are calculated based on the model's (in the ABOT configuration) instantaneously simulated SST and atmospheric variables at each time step. As an approach to restoring SSTs to prescribed values, the partial coupling uses the prescribed SSTs only in the calculation of the heat fluxes driving the atmosphere. The ocean sees the anomalies through the simulated atmospheric variables, which are modulated by the prescribed SSTs.

To keep the seasonal extent of the sea ice as close as possible to BCM_{CTRL} and, thus, to exclude possible remote effects caused by changes in the Arctic and Antarctic sea ice extent, the partial coupling is limited to the region south (north) of the monthly maximum sea ice extent in the Arctic (Antarctic) based on BCM_{CTRL}. The partial coupling is furthermore gradually introduced over a 10° latitudinal band poleward of 25° and a 700-km band equatorward of the monthly maximum sea ice extent.

In addition, a dedicated control experiment ($ABOT_{CTRL}$) is performed as a reference for the ABOT experiment. $ABOT_{CTRL}$ is identical to ABOT except for in the partially coupled region (the extratropics) where the prescribed SSTs that force the atmosphere equal the monthly climatological SSTs extracted from BCM_{CTRL} (and are thus without the 2°C anomaly in ABOT). The motivation for $ABOT_{CTRL}$ is to account for any model drifts that may arise from the partial coupling. Therefore, the difference between $ABOT_{CTRL}$ and BCM_{CTRL} gives a measure of the extent to which the applied partial coupling technique degrades the state of the BCM.

Later on, all of the presented anomalies are derived as the difference between ABOT and $ABOT_{CTRL}$. The partially coupled experiments are run for 100 yr, starting from year 120 of the 300-yr BCM_{CTRL}. It has been confirmed that differences between $ABOT_{CTRL}$ and BCM_{CTRL} are small for all of the analyzed quantities (not shown). This indicates that it is not likely that the applied partial coupling technique degrades the coupled system in significant ways on the temporal and spatial scales considered here.

To the best of our knowledge, the presented study is the first to feature ABOT-type experiments made with a coupled model with an isopycnic coordinate oceanic GCM. Since an isopycnic coordinate oceanic GCM is—by construction—particularly suited for studying oceanic subduction processes (e.g., McDougall 1987), it is believed that the applied system has the ability to add insight to our understanding of the central aspects of the ABOT type of responses.

3. Tropical ocean temperature change

a. Annual-mean SST

The mean BCM_{CTRL} simulated (300 yr) SSTs are slightly low at low latitudes, compared with the Reynolds climatological SSTs. The largest discrepancy from climatology is found in the equatorial Pacific, which is associated with a strong upwelling in the model (cf. Furevik et al. 2003).

In near equilibrium a 2°C SST warming in the extratropics of the world oceans increases the equatorial SST by about 1.5°C (Fig. 1). Regions with SST anomalies exceeding 1.5°C can be seen in the central to eastern equatorial Pacific and, in general, in the eastern subtropical North–South Pacific. Local maximum SST anomalies can also be found in the eastern subtropical South Indian Ocean and in the subtropical South At-

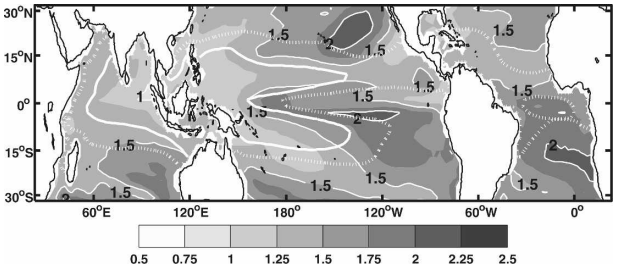

FIG. 1. Annual-mean SST anomalies averaged over years 51–100. Contour intervals are 0.25°C. The white solid (dashed) heavy lines indicate the 27.5°C contour lines for $ABOT_{CTRL}$ (ABOT).

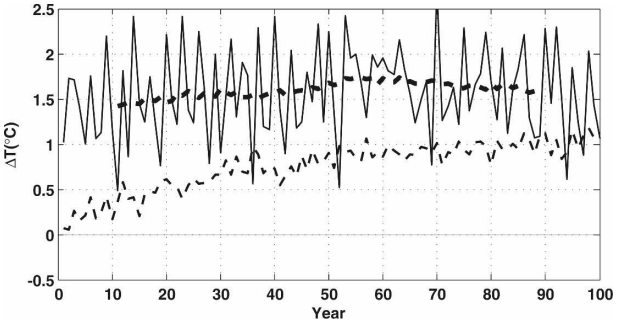

FIG. 2. Evolution of the annual-mean SST anomaly (solid line), its 21-yr running mean (heavy dashed line), and the subsurface (40–400-m average) temperature anomaly (thin dashed line) averaged over the tropical Pacific, between 10°S and 10°N.

lantic. The SST anomalies in the western equatorial Pacific (5°N–5°S, 140°–170°E) and the eastern Pacific (5°N–5°S, 120°–90°W) are 1.4° and 1.6°C, respectively. The west–east SST gradient in the tropical Pacific is thus reduced in ABOT, a pattern similar to the results of coupled GCM simulations forced with increasing greenhouse gas concentrations (e.g., Timmermann et al. 1999). In the Niño-3.4 region (5°N–5°S, 170–20°W), the SST anomalies reach 1.7°C. As expected, the 27.5°C isolines enclose a much larger area in ABOT than in $ABOT_{CTRL}$ (the white heavy lines in Fig. 1).

In a similar sensitivity experiment with prescribed 2°C SST anomalies in the global extratropics, YL05 found that the equatorial SST increased with about 1°C, which is less than the anomaly presented here. This discrepancy may be due to different descriptions of the dynamics and thermodynamics processes by the two climate models, especially in the ocean components. In YL05, the prescribed ocean temperature anomaly in the region of partial coupling is distributed over the uppermost 20 m of the oceanic GCM [the Geophysical Fluid Dynamics Laboratory's z-level Modular Ocean Model, (GFDL-MOM)]. In contrast, the prescribed ocean temperature is absorbed over the whole surface mixed layer in MICOM. Since the surface mixed layer depth in the extratropics is usually close to or in excess of 100 m, the surface heat content anomaly is likely larger in MICOM than that is in GFDL-MOM, given the same imposed SST anomaly. Hence, in MICOM, the anomalous warmed mixed layer water in the extratropics can release more heat into the tropics during the process of heat exchanges between the two regions and, hence, strengthen the extratropical forcing on the tropics.

b. Evolution of tropical temperature anomalies

The equatorial Pacific SST increases by 1.0°C only after a few years (Fig. 2). The equatorial Pacific SST anomaly reaches a near-stable equilibrium after about 20 yr. For the final 50 yr, the SST anomaly in the equatorial Pacific is about 1.6°C, with a standard deviation of 0.3°C. Since the ocean and atmosphere are fully coupled in the global tropics, the interannual ENSO signal can still be represented in ABOT, with a frequency of about 3 yr, which is close to that in BCM_{CTRL} (cf. Furevik et al. 2003; Zhou et al. 2006b).

In contrast to the rapid adjustment of the SST, the subsurface (40–400 m) temperature in the tropical Pacific shows a large delay response. The equatorial Pacific subsurface temperature increases gradually over the first 50 yr, and has an anomaly of about 0.7°C around year 40 (Fig. 2). In the following 50 yr, the equatorial subsurface temperature continues to increase and reaches a relative stable state with an anomaly of 1.0°C.

The rapid changes in SST should be achieved by the quick atmospheric bridge, while the delayed response in the subsurface temperature is related to the slow ocean adjustment (e.g., YL05, Wu et al. 2007). The slow adjustment processes of the subsurface temperature will be described in more detail in section 5c.

c. Changes in surface winds and ocean currents

The annual-mean surface winds in the Pacific are dominated by the trade winds (Fig. 3b). The easterly trade winds converge in the region of the ITCZ in the North Pacific and the South Pacific convergence zone in the South Pacific. The zonal trade winds are reduced by about 0.5 m s^{-1} in ABOT (Fig. 3a). The largest anomalies are found in two regions: one extending southeastward from the warm pool at about 150°E to the subtropical southeast Pacific, and the other extending along about 15°N in the central subtropical North Pacific.

The simulated mean ocean surface current in $ABOT_{CTRL}$ (Fig. 3d) shares a similarity with previous

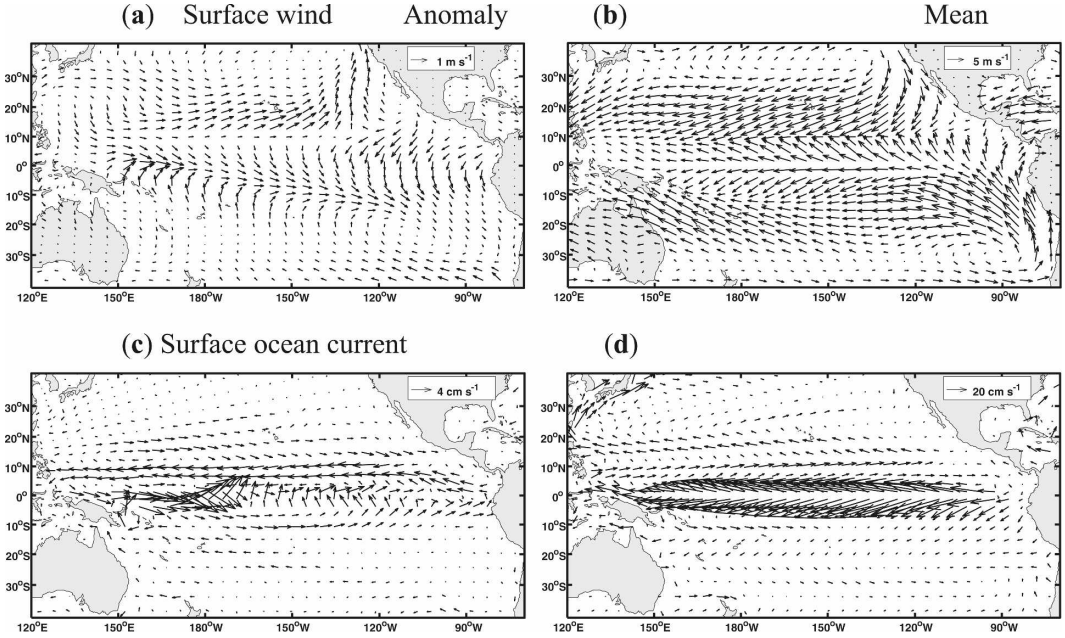

FIG. 3. The anomalies of (a) annual-mean surface wind and (c) surface ocean current. (b), (d) As in (a), (c) but for the corresponding annual-mean climatologies.

results (e.g., Bonjean and Lagerloef 2002): The South Equatorial Current (SEC) occupies the whole equatorial Pacific, riding the equator with a meridional width of about 10°. The weaker North Equatorial Current (NEC) shows up between 20° and 10°N. Between the SEC and the NEC, there is the North Equatorial Counter Current, along roughly 8°N. The weak South Equatorial Counter Current can also be seen on the southern flank of the SEC, extending along 10°S from 160°E to 150°W. In ABOT, the SEC is generally reduced by about 2 cm s^{-1} (Fig. 3c). For the meridional velocity component, the largest anomaly appears just south of the equator from 160° to 110°W, indicating a weakened poleward transport of equatorial surface water. As a consequence, the poleward heat transport is reduced and more heat is stored in the equatorial region, favoring a local maximum warming there (Fig. 1).

4. Heat balance

a. Surface heat budget

The main surface heat fluxes into the ocean are downward shortwave radiation (Q_{SW}), downward minus upward longwave radiation (Q_{LW}), and upward latent heat (Q_{Lat}). The sensible heat flux (Q_{Sens}), governed by the temperature difference across the air–sea interface, is directed upward and is relatively small in the equatorial Pacific (Fig. 4b). Similarly, the net longwave radiation is also directed upward. The major contributor for the net downward heat flux (Q_{Net}) is thus the surface shortwave heat flux.

The net downward surface heat flux in the equatorial Pacific is reduced in ABOT ($Q'_{Net} < 0$; Fig. 4a, positive downward). The main contributor to this reduction is the enhanced upward surface latent heat flux ($Q'_{Lat} < 0$), corresponding to increased evaporation. Although the surface wind is weakened, the warmer surface temperatures lead to a saturated vapor pressure increase (with a relative value larger than 11%), which favors enhanced surface latent flux. Because the increase of the surface air temperature (1.58°C) is larger than that of the SST (1.52°C) in the equatorial Pacific, the net longwave radiation anomaly ($Q'_{LW} > 0$) and the sensible heat flux anomaly ($Q'_{Sens} > 0$) are both downward, warming the sea surface layer. The surface air temperature anomalies in the deep tropics are connected with positive temperature anomalies in the subtropics in the lower troposphere (not shown), implying anomalous advections of warm air from the subtropics by the trade winds. The warming amplification in the upper troposphere in the tropics (not shown) can also contribute to the surface air warming through downward heat flux. The anomaly of the net surface shortwave radiation is small and downward ($Q'_{SW} > 0$), mainly due to the weak reduction in the total cloud cover (−0.4%) from its mean value of 68.4%.

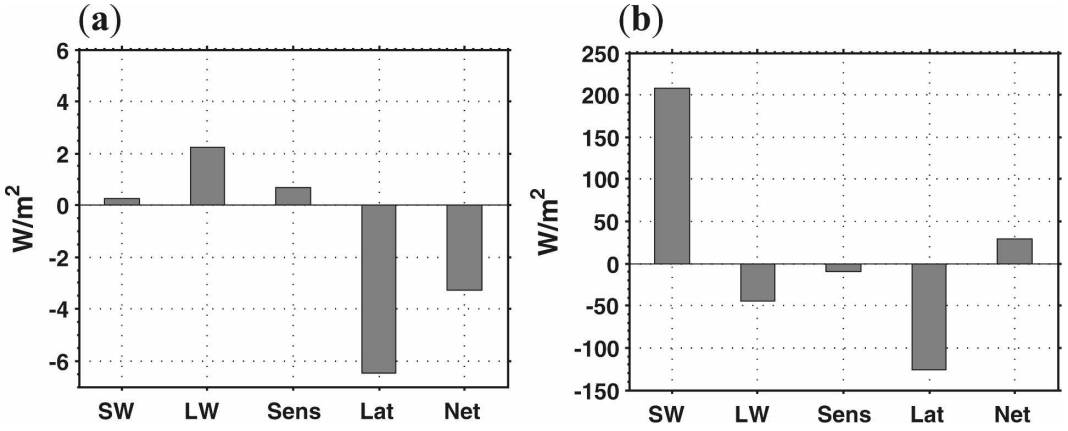

FIG. 4. The surface heat budget anomalies (a) in the equatorial Pacific (10°N–10°S, 130°E–90°W) averaged over years 51–100. (b) The mean values in $ABOT_{CTRL}$. Shown are SW, the net surface shortwave radiation; LW, the surface longwave radiation; Sens, the surface sensible heat flux; Lat, the surface latent heat flux; and Net, the net surface heat flux. All values are positive downward.

b. Surface heat balance

In addition to the air–sea exchange of heat, there are heat fluxes associated with horizontal and vertical advection and diffusion in the ocean. The equation for the SST tendency can be diagnosed using monthly mean fields interpolated to fixed depths following the equation $(\partial T/\partial t) = (Q_{\mathrm{Net}}/\rho C_p h) - uT_x - \upsilon T_y - wT_z + \mathrm{Residual}$. Here ρ is the seawater density, C_p is the heat capacity of seawater, and, for diagnostic purposes, $h = 40$ m can be taken as the thickness of the surface mixed layer in the equatorial Pacific. The difference between the actual and diagnosed evolutions of SST equals the residual term, which contains the diffusion and mixing. Similarly, the anomalous SST tendency equation can be put in the form of $(\partial T'/\partial t) = (Q'_{\mathrm{Net}}/\rho C_p h) - (uT_x)' - (\upsilon T_y)' - (wT_z)' + (\mathrm{Residual})'$, where primes denote the anomalies.

For $ABOT_{CTRL}$ (Fig. 5b), it follows that cool waters below the mixed layer are upwelled to the surface ($-wT_z < 0$; e.g., for z is positive upward, $w > 0$, $T_z > 0$; thus, $-wT_z < 0$) and are subsequently warmed by the net surface heat flux ($Q_{\mathrm{Net}} > 0$). The cold water in the equatorial upwelling region is transported poleward by the mean Ekman current ($-\upsilon T_y < 0$; e.g., north of the equator, $\upsilon > 0$, $T_y > 0$; thus, $-\upsilon T_y < 0$) and transported westward by the SEC ($-uT_x < 0$; $u < 0$, $T_x < 0$; thus, $-uT_x < 0$).

In ABOT (Fig. 5a), the anomalous warm SST is maintained by dynamics different from that of $ABOT_{CTRL}$. The anomalous net surface heat flux is negative ($Q'_{\mathrm{Net}} < 0$), tending to reduce the SST in the

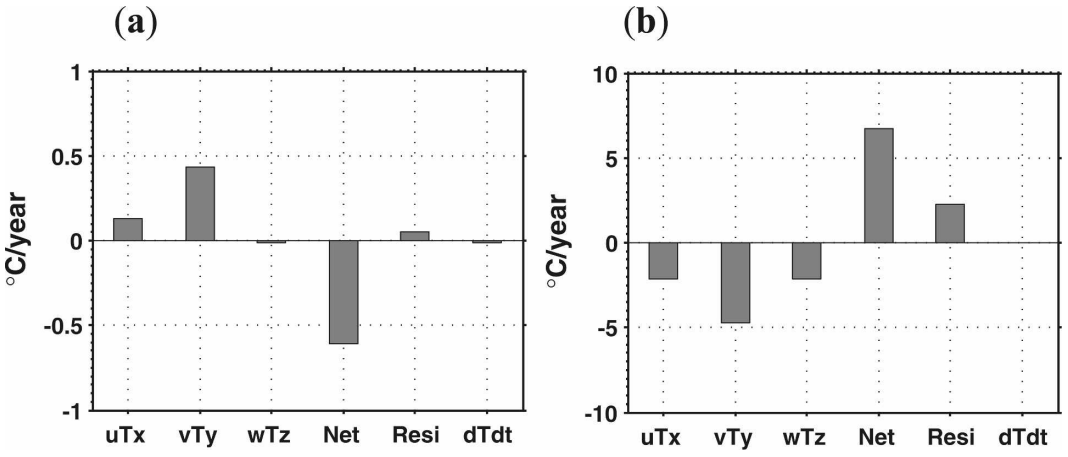

FIG. 5. The heat balance anomalies (a) averaged over a 40-m-thick surface box in the equatorial Pacific (10°N–10°S, 130°E–90°W) over years 51–100. (b) The corresponding mean values in $ABOT_{CTRL}$. From left to right, the terms are $-uT_x$, $-\upsilon T_y$, $-wT_z$, $(Q_{\mathrm{Net}}/\rho C_p h)$, the residual term, and $(\partial T/\partial t)$.

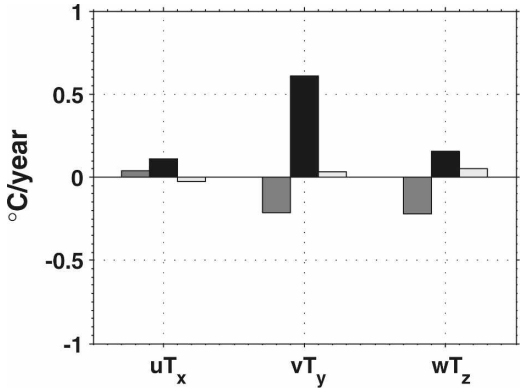

FIG. 6. Decomposition of the temperature advection anomaly averaged over a 40-m-thick surface box in the equatorial Pacific (10°N–10°S, 130°E–90°W) over years 51–100. From left to right, three clusters of bars represent the mean advection term, the perturbation advection term, and the nonlinear term; e.g., $-(uT_x)' = -uT'_x - u'T_x - u'T'_x$ for $-(uT_x)'$, $-(vT_y)'$, and $-(wT_z)'$.

equatorial Pacific. The positive SST response is mainly favored by the positive meridional convergence of the heat transport ($-(vT_y)' > 0$). In addition, the contribution of the zonal convergence of the heat transport ($-(uT_x)' > 0$) to the positive SST anomaly reaches up to 20% of the positive SST trend.

The temperature advection anomaly in the ocean can be further decomposed into three parts: the first-order mean advection and perturbation advection terms, and the nonlinear (second order) term [e.g., $-(uT_x)' = -uT'_x - u'T_x - u'T'_x$]. The contributions from each of the three terms are displayed in Fig. 6. The nonlinear terms are relatively small and are therefore neglected in the following discussion.

The meridional heat transport anomaly is dominated by the weakened poleward transport ($-v'T_y > 0$; e.g., north of the equator, $v' < 0$, $T_y > 0$; thus, $-v'T_y > 0$). The positive SST anomalies have a local maximum south of the equator (about 5°S) in the central Pacific (Fig. 1), reducing the meridional temperature gradients on the southern flank of the equator. The localized maximum SST anomalies south of the equator make a negative contribution to the heat convergence ($-vT'_y < 0$; e.g., south of the equator, $v < 0$, $T'_y > 0$; thus, $-vT'_y < 0$).

Corresponding to the reduction of the SEC, the westward heat transport is weakened, leading to a positive heat convergence in the equatorial Pacific ($-u'T_x > 0$; $u' > 0$, $T_x < 0$; thus, $-u'T_x > 0$). The zonal SST anomaly gradient is positive (Fig. 1), and also favors the heat convergence ($-uT'_x > 0$; $u < 0$, $T'_x > 0$; thus, $-uT'_x > 0$). In YL05, the contribution of $(uT_x)'$ is slightly smaller than that in our results. The zonal SST anomaly gradient is negative in YL05, and the $-uT'_x$ term is negative, canceling out the positive contribution of the term $-u'T_x$.

Weakened easterlies near the equator result in reduced upwelling in the tropical Pacific, from 20.1 Sv (1 Sv = 10^6 m^3 s^{-1}) in $\text{ABOT}_{\text{CTRL}}$ to 18.3 Sv in ABOT, making a positive contribution to the heat convergence ($-w'T_z > 0$; e.g., for z is positive upward, $w' < 0$, $T_z > 0$; thus, $-w'T_z > 0$) in the surface ocean layer. Although there is a positive anomaly of the subsurface ocean temperature in ABOT, its amplitude is less than that of the SST. Hence, the vertical temperature gradient anomaly is positive (for z is positive upward, $T'_z > 0$), and its contribution to the heat convergence in the surface ocean layer is negative ($-wT'_z < 0$; $w > 0$, $T'_z > 0$; thus, $-wT'_z < 0$).

5. Circulation dynamics

In the previous section, it is seen that the ocean meridional advection plays a major role in maintaining the SST anomaly in the equatorial Pacific. In this section, the dynamics of the changes in the ocean circulation, as well in as the atmosphere circulation, are investigated.

a. Atmosphere circulation

The annual-mean Hadley circulation in ABOT is weakened and the magnitude of the anomalies is typically up to 10% of that of $\text{ABOT}_{\text{CTRL}}$ (Fig. 7). The streamfunction anomaly is nonsymmetric across the equator, with positive values between about 20°S and 15°N, small or vanishing anomalies poleward of 15°N, and a localized negative cell between 40° and 25°S. A maximum positive anomaly is found at the equator (Fig. 7a), indicating that the ascending motion there (Fig. 7b) is reduced. At 20°S, the descending motion is reduced in ABOT, whereas at 10°N, the ascending motion is reduced.

Since the Hadley cells are mostly thermally driven (Holton 2004) and the convective motions are associated with divergence, the divergent winds are used to diagnose the relationship between convection anomalies and atmosphere circulation anomalies. Horizontal wind velocity V can be split into a nondivergent (rotational) part and a divergent (irrotational) part: $V = V_\psi + V_\phi = \mathrm{k} \times \nabla\psi + \nabla\phi$, where ψ is the streamfunction and ϕ is the velocity potential. By definition, the divergent wind flows from low centers to high centers of the velocity potential field.

In the annual-mean velocity potential at 200 hPa (not shown), there is a center of divergence in the western equatorial Pacific and two centers of convergence, one in the subtropical southeastern Pacific and another in the tropical South Atlantic. Corresponding to the di-

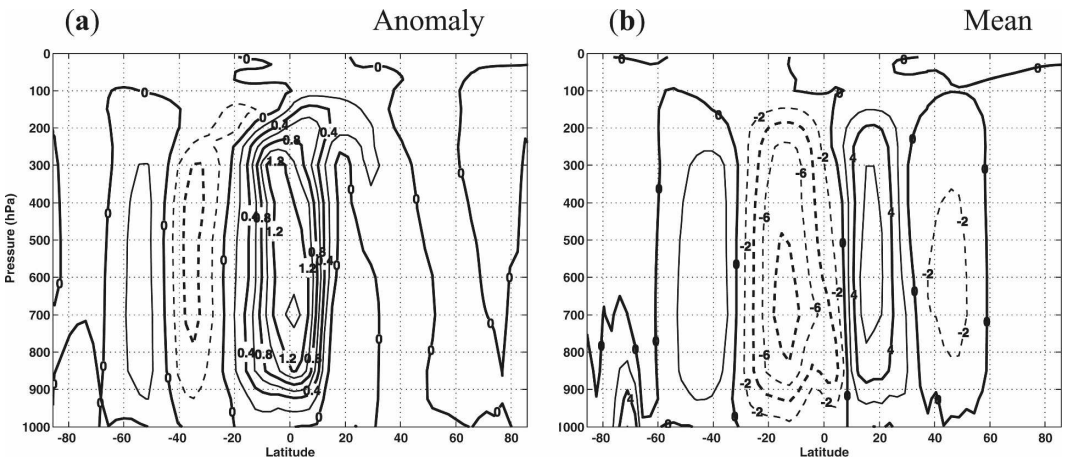

FIG. 7. (a) Anomalous and (b) mean meridional streamfunctions of the global atmosphere over years 51–100. Contour intervals are 0.2×10^{10} kg s^{-1} in (a) and 2×10^{10} kg s^{-1} in (b).

vergence (convergence) at 200 hPa, there are convergence (divergence) centers at 850 hPa (not shown). The Walker circulation is well defined by the centers of the upward motion around the western Pacific warm pool and the downward motion at the eastern Pacific and the Atlantic. All of these features are consistent with previous results based on reanalysis data (e.g., Wang 2002).

Together with the reduced Hadley circulation, the Walker circulation is also weakened, which can be seen from the fields of the velocity potential and the divergent wind (Figs. 8a and 8b). There are negative velocity potential anomalies at 200 hPa (Fig. 8a) in the tropical South Pacific (around 140°W) and in the tropical South Atlantic (around 20°W), and positive anomalies over the southeast Asia region (around 10°N, 100°E). Corresponding to these negative (positive) velocity potential anomalies at 200 hPa, there are positive (negative) anomalies of the velocity potential at 850 hPa (Fig. 8b). The anomalous upper-tropospheric divergences in the tropical South Pacific and the tropical South Atlantic are situated at the locations of positive precipitation anomalies (Fig. 8c), while the center of the upper-tropospheric convergence anomaly in southeast Asia is located in the region of negative precipitation anomalies (Fig. 8c).

The regions of the above-mentioned enhanced convection are primarily located south of the equator, at around 5°S in the South Pacific and around 10°S in the South Atlantic. The reduced convection occurs north of the equator with its center around 10°N in southeast Asia. Enhanced convection in the Southern Hemisphere and reduced convection in the Northern Hemisphere together construct a pattern of a positive streamfunction anomaly, representing a weakened Hadley circulation anomaly (Fig. 7a). In the tropical Pacific, the convection is reduced in the west and enhanced in the east, which favors a weakened Walker circulation, consistent with anomalous westerly winds at the surface (Fig. 3a). As a whole, the ITCZ shifts southward in all three ocean basins and eastward in the Pacific, which is reflected by the changes both in the three-dimensional atmospheric circulation and the large-scale convective precipitation distribution.

Related to the large-scale redistribution of the precipitation, the atmospheric moisture transports show some apparent changes. In the tropics, the annual-mean atmospheric circulation transports moisture from the Atlantic and Indian basins into the Pacific basin (gray vectors in Fig. 8d), providing a necessary water source for the formation of the convective precipitation in the ITCZ. In ABOT, the moisture transports from the Atlantic to the Pacific are enhanced (Fig. 8d). After passing over the landmass of the Americas the anomalous moisture transports point to the anomalous convection (around 10°S and 140°W) in the tropical South Pacific. The moisture transport anomalies converge in the regions around the enhanced convection anomalies. The convergence of the anomalous moisture transport also occurs in other anomalously enhanced convection regions, for example, the tropical South Atlantic and the eastern South Indian Basin.

Since the water vapor acts as "fuel" in the formation of deep convection, the changes in moisture transport play a key role in the redistribution of convective precipitation. Although the evaporation is enhanced in the tropical oceans in ABOT, the evaporation anomalies cannot locally support the anomalous precipitation (not shown). A large part of the vapor supply for the enhanced convection anomalies is provided by anomalous moisture transports from surrounding regions. The

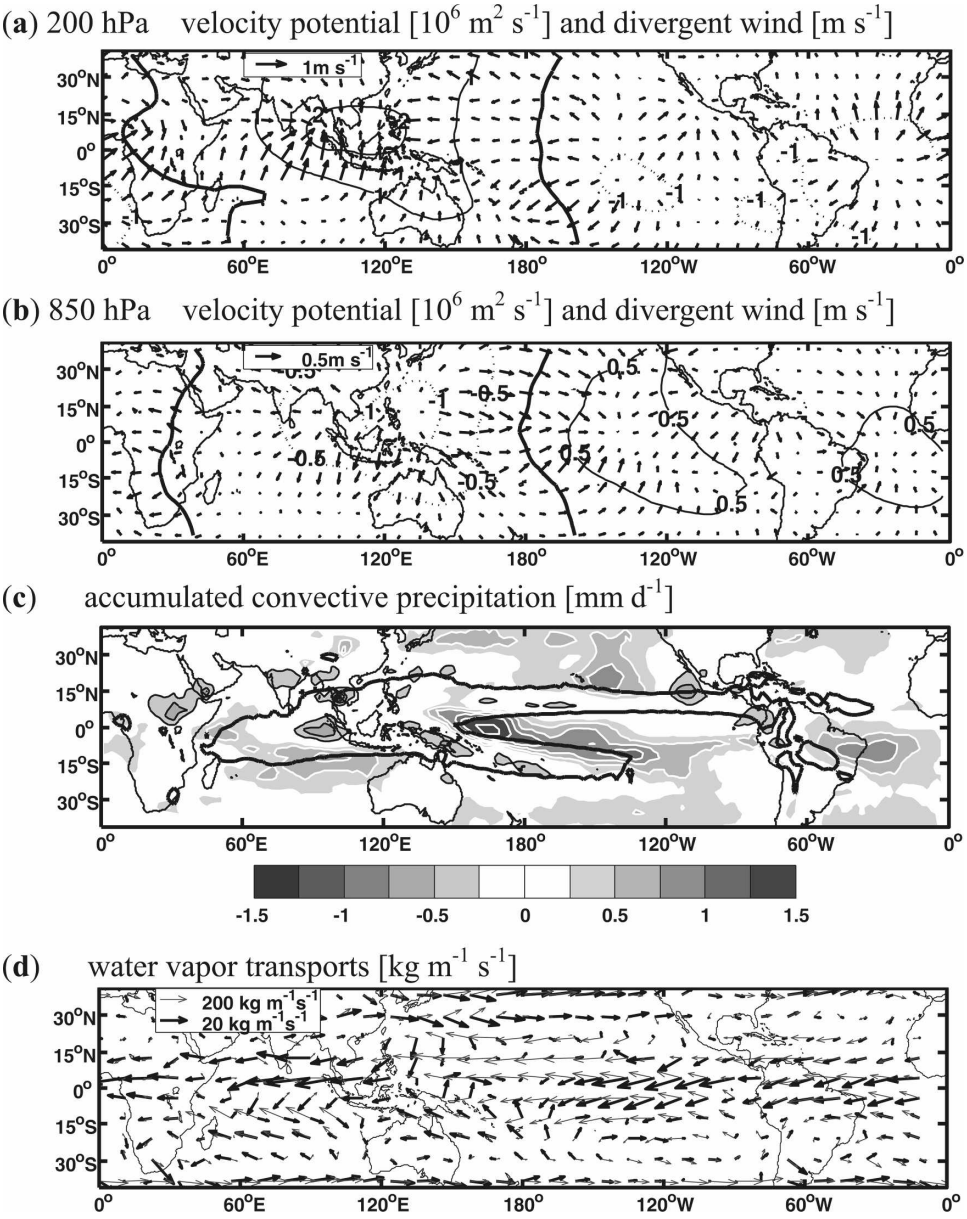

FIG. 8. The atmospheric fields related to the convection anomalies in the tropical Pacific over years 50–100. (a) The anomalous velocity potential (contours, with intervals of 0.5×10^6 m^2 s^{-1}) and divergent wind (vectors, in m s^{-1}) at 200 hPa. (b) Same as in (a) but at 850 hPa. (c) The anomalous accumulated convective precipitation [in mm day^{-1}, positive downward, the shadings with white (black) contour lines indicate positive (negative) values; solid black lines are the contour lines of 5 mm day^{-1} in ABOT$_{CTRL}$, representing the mean location of the ITCZ]. (d) Water vapor transports below 400 hPa (in kg m^{-1} s^{-1}, the gray vectors represent the values in ABOT$_{CTRL}$).

moisture transport anomalies are caused by two factors: One is the increased capacity of the atmosphere to retain water vapor due to higher air temperatures; the other is the anomalous atmospheric circulation. Far away from the anomalous convection regions, the anomalous moisture transports are approximately along the direction of the mean atmospheric circulation, implying that enhanced relative humidity plays a major role in the moisture transport changes. The contribution of atmospheric circulation anomalies to moisture transport becomes important in the regions near the convection anomalies, which is shown by the convergent pattern of the anomalous water vapor transport vectors there (Fig. 8d).

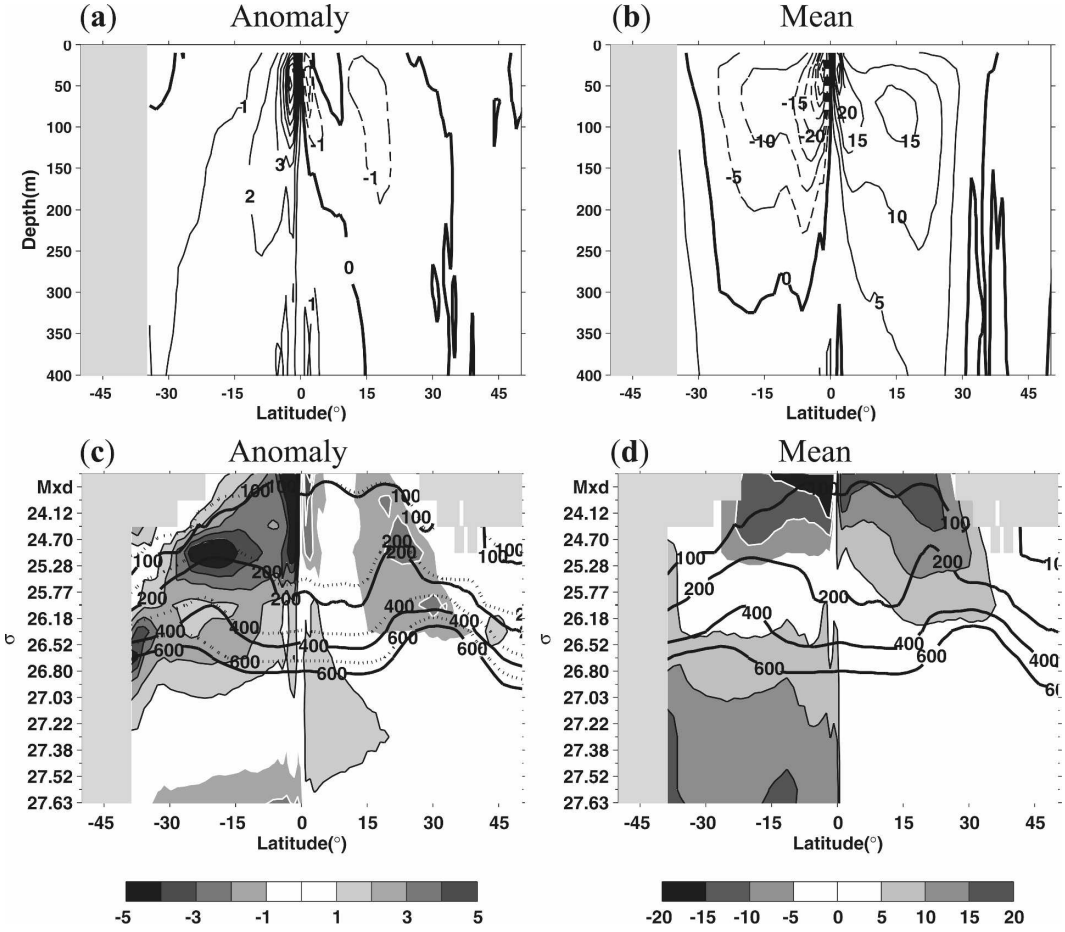

FIG. 9. The anomalous meridional overturning streamfunction in the Pacific basin (without the Indonesian Throughflow) as a function of (a) depth and (c) vertical density. (b), (d) As in (a), (c) but for the corresponding values from the $ABOT_{CTRL}$ climatologies. The depths (m) of the isopycnals from $ABOT_{CTRL}$ (ABOT) are imposed as solid (dashed) lines in (c), (d). Contour intervals are 1 Sv (1 Sv=10^6 m^3 s^{-1}) in (a), (c) and 5 Sv in (b), (d). The shading with black (white) contour lines indicates positive (negative) values in (c), (d).

A common feature of the convection anomalies is that they generally are located at the climatological ITCZ boundary (the solid black lines in Fig. 8c), on the main moisture transport paths directed to the climatological convection centers (gray vectors in Fig. 8d), and on the edge of the warm pool in ABOT (enclosed by 27.5°C contours, white dashed heavy lines in Fig. 1). After the ocean becomes warmer, SSTs in some regions rise up to the threshold for the generation of deep convective activity [about 27.5°C; Graham and Barnett (1987)], which occurs mainly near the boundary of the warm pool and the ITCZ. When there is adequate water vapor, which can be easily met on the main paths of the climatological moisture transport, warmer SSTs above the threshold help anomalous convection come into being. From the view of the moisture transport path, the convection anomalies are present on the downstream of the local maximum SST anomalies (Figs. 8d and 1). The warmer SSTs favor higher evaporation, which is readily transported downstream to fuel the anomalous convection.

Once the anomalous convections are set up on the main paths of the moisture transport, they consume a considerable part of the water vapor, which "should" be transported into the mean convection centers in climatology. Since the water vapor supply is cut off halfway, the climatological convection activities are suppressed, which is indicated by a reduction in the convective precipitation, for example, in the southeast Asia region (Fig. 8c).

b. *Ocean circulation*

The ocean meridional streamfunction (Fig. 9b) in the $ABOT_{CTRL}$ shows that the Pacific STCs have features that are consistent with prior studies (e.g., Liu et al. 1994; Capotondi et al. 2005). Subtropical waters are

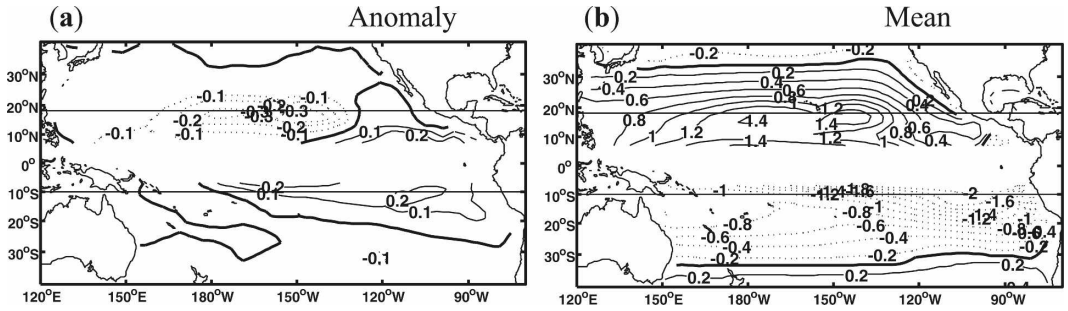

FIG. 10. (a) Anomalous and (b) mean meridional Ekman volume transport per unit length over years 51–100. Contour intervals are 0.1 $m^2 s^{-1}$ in (a) and 0.2 $m^2 s^{-1}$ in (b). Values are positive northward.

subducted in the regions of downward Ekman pumping (around 15°–30°S and 15°–30°N). The subducted waters then flow equatorward over the uppermost 100–400 m of the water column (Fig. 9b), or at isopycnals extending down to $\sigma_0 = 26.2$ in the North Pacific and to $\sigma_0 = 25.28$ in the South Pacific (Fig. 9d). The subducted waters return to the surface at the equator and are thereafter forced poleward by Ekman divergence. The streamfunction isoline of 5 Sv reaches more than 400 m in the North Pacific, but only at 200 m in the South Pacific, shallower than previous model results (e.g., Capotondi et al. 2005).

It should be noted that there are also signatures of tropical cells (TCs) present in the annual-mean streamfunction. Parts of the poleward-directed surface water sink within 7°S and 7°N, forming a closed cell on each side of the equator. This phenomenon is seen as a function of both depth (Fig. 9b) and vertical density (Fig. 9d). The presence of the TCs has been reported in numerous observation and model-based studies (e.g., Philander et al. 1987; Kessler et al. 1998; Schott et al. 2004; Lohmann and Latif 2005).

In ABOT, the strength of the annual-mean STCs in the Pacific is reduced by more than 1 Sv in both hemispheres (Fig. 9a). Apparent anomalies of the shallow (0–200 m) meridional overturning circulation are related to the TCs near the equator, reaching up to about 2 Sv. The strong TC reduction is driven predominately by the local equatorial westerly anomalies (Fig. 3a). A maximum streamfunction anomaly on the isopycnal layers (Fig. 9c) is found in the South Pacific, around 20°S, but there is no such signal in the pattern as a function of depth (Fig. 9a). This streamfunction anomaly on isopycnals is caused by a distinct increase in the layer thickness of the isopycnal $\sigma_0 = 25.28$ there. Although the meridional velocities of the same layer are reduced (not shown), the volume transport on the isopycnal there is enhanced due to an increased layer thickness.

McCreary and Lu (1994) found that the strength of the STCs can be diagnosed based on the zonal wind stress τ^x and the Coriolis parameter f at fixed latitude, or equally on the magnitude of the meridional Ekman volume transport, $M_e^y = -(\tau^x/\rho f)$. Hence, the change of modeled STCs may be related to the change of the theoretical Ekman transport.

The annual-mean and anomalous meridional Ekman transports are shown in Fig. 10. Two strong Ekman transport anomalies can be seen (Fig. 10a): one in the subtropical North Pacific along 18°N, with a zonal extent of more than 6000 km, and another in the eastern tropical South Pacific at about 10°S. We will focus on these two latitude bands to describe the strongest anomalies in the Ekman transports. Since the TC convergences occur primarily within 7° of the equator (Schott et al. 2004; Fig. 9b), the latitudinal bands at 10°S and 18°N do not involve the TCs. At latitudes of 10°S and 18°N, positive values of zonally integrated poleward transports are only present in the surface mixed layer. Hence, the index for the strength of the modeled STCs surface branch can be simply defined as the strength of the zonally integrated meridional transport in the surface mixed layer. Similarly, the index of the meridional theoretical Ekman transport is calculated as the zonally integrated meridional Ekman volume transports at 10°S and 18°N.

For $ABOT_{CTRL}$, the final 50-yr mean of the zonally integrated poleward Ekman transports along 10°S (18°N) is 19.3 Sv (15.6 Sv), and the zonally integrated poleward volume transports in the surface mixed layer in MICOM along 10°S (18°N) are 19.2 Sv (19.1 Sv). Thus, the theoretical Ekman transport dominates the simulated meridional mixed layer transport at 10°S. At 18°N, the simulated meridional transport in the mixed layer exceeds the Ekman transport by about 3.5 Sv. In ABOT, the zonally integrated poleward Ekman transports at 10°S (18°N) are reduced by 1.4 Sv (1.8 Sv), whereas the corresponding values for the simulated

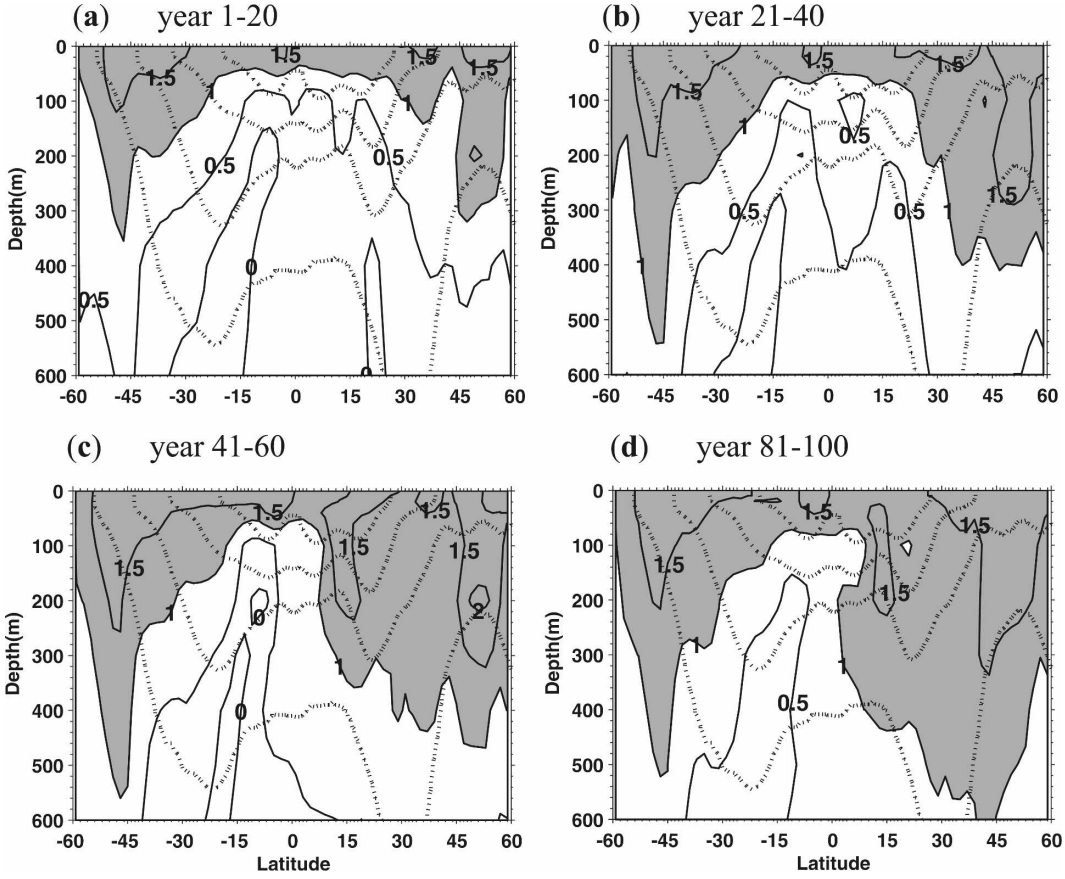

FIG. 11. Zonal-mean Pacific Ocean temperature anomalies averaged over every 20 yr. (a)–(d) Results are shown for four time periods to demonstrate the development. The contour lines are shaded for absolute temperature anomalies larger than 1.0°C. The climatological zonal-mean depths of isopycnals σ_0 = 24.12, 25.28, 26.18, and 26.8 from $ABOT_{CTRL}$ are superposed as thick dashed lines.

poleward volume transports in the surface mixed layer are 2.6 Sv (1.4 Sv). Therefore, the reduced strength of the STCs' surface branch can be largely ascribed to changes in Ekman transports and, furthermore, to changes in the zonal surface winds.

A weakening of the STCs reduces the heat exchange between the tropics and the extratropics, and hence sustains the tropical warming (McPhaden and Zhang 2002; YL05; Wu et al. 2007). Since the global SST and surface wind reach quasi equilibrium within one decade, the STCs reach a nearly stable state in around two decades (not shown). On the other hand, the subsurface temperature in the tropical Pacific shows a large delay response, with a time scale larger than five decades (Fig. 2). Hence, a detailed description of the subsurface temperature evolution is desired.

c. Subsurface temperature anomalies

The processes regarding the ocean tunnel can be inferred by the subsurface temperature evolution (Fig. 11). In the first 20 yr, the positive anomalies of the zonal-mean sea temperature appear in the uppermost 100 m in the tropical Pacific, with a maximum value of 1.5°C in the mixed layer south of the equator (Fig. 11a). The tropical temperature anomalies are connected with the extratropical temperate anomalies in the upper mixed layer. In the following 20 yr, the tropical ocean temperatures continue to increase (Fig. 11b). The 1.0°C temperature anomaly reaches a depth of about 80 m in the tropics. The subducted positive extratropical temperature anomalies continue to extend equatorward primarily along isopycnals. For example, the anomaly of 1.0°C on isopycnals around σ_0 = 26 reaches 30°S. In the third 20 yr, the ocean temperature changes occur primarily in the North Pacific (Fig. 11c), and the signals of the 1.0°C anomaly on the isopycnals around σ_0 = 26 reach 10°N. In the final quasi-equilibrium state, the subsurface temperature 1.0°C anomalies from the North Pacific arrive at the equator (Fig. 11d). During the whole period, the maximum SST anomalies near

the equator gradually become slightly larger, suggesting a certain contribution from the subsurface anomalies through upwelling and mixing.

The tardy subsurface response in the tropical Pacific (mentioned in section 3b) can be traced to the extratropical Pacific basin. In the extratropics, the imposed temperature anomalies on the surface penetrate into subsurface gradually. In the South Pacific, the 1.5°C anomaly isoline arrives at a depth of 100 m or above the isopycnal $\sigma_0 = 26.8$ in the first 20 yr (Fig. 11a). In the following periods, the 1.5°C anomaly appears at a depth of 200 m (Fig. 11b). In the North Pacific, the 1.5°C anomaly can be found only in the upper 50 m in the fist 20 yr (Fig. 11a). The 1.5°C anomaly continues to penetrate downward onto the isopycnal $\sigma_0 = 26.8$ and extend to a larger area (Fig. 11b). In addition to the subduction process on a certain isopycnal, the dipycnal mixing as well as the ocean dynamics adjustment in the local basins (on several decades) may also be responsible for the slow subsurface changing in the extratropics. Hence, although the STCs reach quasi equilibrium within two decades, the slow subsurface warming in the extratropics and its equatorward intrusion can lead to the large delay in the tropical subsurface temperature response on time scale of several decades.

After forming in the extratropics, the temperature anomalies move equatorward mostly along isopycnals. The time scale for the extratropical anomalies arriving at the deep tropics is about one to two decades, which can be indicated by the movement of the 1.0°C anomaly isoline along the isopycnal $\sigma_0 = 26.18$ from about 30°N in the second 20 yr (Fig. 11b) to about 12°N in the third 20 yr (Fig. 11c). This time scale for extratropical anomaly intrusion into the tropics is consistent with previous results (e.g., Schott et al. 2004). A notable feature is that the equatorward intrusion of subsurface temperature anomalies from the South Pacific is blocked at around 18°S. This local minimum temperature anomaly in the subtropical South Pacific is accompanied by negative salinity anomalies. The relation between the anomalies of temperature and salinity can be clearly displayed by their horizontal patterns.

Compared with $ABOT_{CTRL}$, the upper-ocean temperature in ABOT depth levels rises in the entire global ocean basin (not shown). On the other hand, the temperature anomalies on a time-dependent isopycnal layer (Fig. 12a) show a distinct discrepancy. Although positive anomalies appear in the mean interior route of the subducted water from the eastern North/South Pacific Ocean basin, they decay gradually on their equatorial way. In the Pacific basin, the positive temperature anomalies cease at latitudes of around 15°N/S. The equatorial Pacific regions are dominated by negative temperature anomalies. In the eastern equatorial Pacific, the negative temperature anomalies reach up to 1.5°C. Similar negative temperature anomalies were also found by Yang et al. (2005) north of the equator and were considered to play a role in blocking advection of the warming anomalies from the North Pacific subtropics to the tropics. The negative temperature anomalies cannot be found on the depth levels in this study. Hence, the deepening of the pycnocline is the primary cause of the negative temperature anomalies in the equatorial Pacific in ABOT.

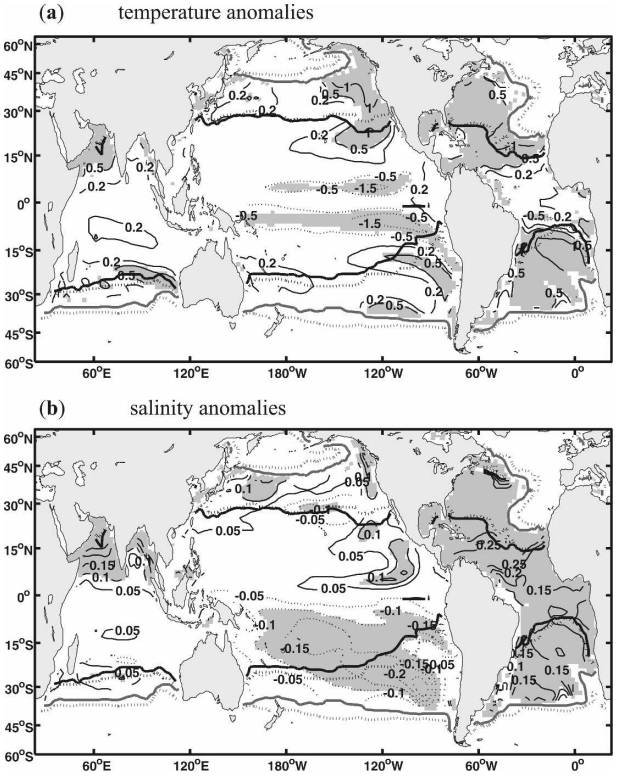

FIG. 12. Annual-mean (a) potential temperature anomalies and (b) salinity anomalies on the isopycnal layers $\sigma_0 = 24.12 - 26.18$, averaged over years 51–100. Units are °C in (a) and psu in (b). The contour lines are shaded for absolute temperature anomalies larger than 0.5°C in (a) and absolute salinity anomalies larger than 0.1 psu in (b). The heavy solid (dashed) lines indicate the outcropping lines of the isopycnal layers $\sigma_0 = 24.12$ from $ABOT_{CTRL}$ (ABOT). Black (gray) lines are given for winter (summer) for each hemisphere.

In addition to the temperature, the salinity can also indicate the ocean circulation direction. In ABOT, the large-sale redistribution of the freshwater contents is changed (not shown). These changes include positive salinity trends in the global subtropics, and freshening trends in the subpolar ocean basins, similar to the salinity changes in experiments with increasing greenhouse gas concentrations (Bethke et al. 2006). Consis-

tent with the results of greenhouse gas experiments, some indirect salinity measurements indicate that freshening of surface waters has occurred in the high-latitude North Pacific and Southern Oceans over the past several decades (e.g., Wong et al. 1999). In the subsurface layer, some salinity anomalies (Fig. 12b) can be found to be associated with certain temperature anomalies (Fig. 12a). In the subtropical northeastern Pacific, there are positive salinity anomalies on the isopycnal layer, around 15°N, in the southwestward route of subducted water originating from the Californian coast. These salinity anomalies share a similar pattern with the positive temperature anomalies there (Fig. 12a). In contrast to the North Pacific, the South Pacific basin is dominated by negative salinity anomalies. The freshening signals follow the mean route of the subsurface water after subduction in the Southern Ocean. Since the surface water becomes fresher in the subpolar region in ABOT (cf. Fig. 1 of Bethke et al. 2006), the waters subducted in the Southern Ocean carry negative salinity anomalies. Due to the compensation of temperature and salinity on certain isopycnal, the subsurface temperature anomalies are largely negative in the subtropical southern Pacific, accompanied by the strong negative salinity anomalies there (Fig. 12).

When outcropping, the isopycnal layer is connected with the surface mixed layer and, therefore, exposed to atmospheric forcing directly. Due to the warming of seawater in ABOT, the density of the surface mixed layer becomes smaller in the extratropics. Another factor reducing the seawater density is the freshening in the subpolar oceans. As a result, the outcropping lines of certain isopycnal layers move accordingly poleward in ABOT (heavy solid–dashed lines in Fig. 12). Generally, the mixed layer temperatures reduce gradually poleward in climatology. Hence, the temperature anomalies actually "seen" by the ventilated isopycnal layers in ABOT are relatively smaller than the prescribed values. As a result, although a temperature anomaly of 2°C is prescribed in ABOT, the anomalous temperature signal subducted into a certain isopycnal layer is weaker than 2°C.

6. Discussion and conclusions

Numerical experiments with the fully coupled Bergen Climate Model using the so-called partial coupling have been carried out to elucidate the climatic impact of the extratropics on the tropics. The main simulated results of our experiments are consistent with those of YL05. For instance, after SST anomalies are imposed in the extratropics, the tropical SSTs rise rapidly and reach a quasi-equilibrium state within several years. However, the tropical subsurface temperatures show a slow response. The fast changes in SST should be achieved by the quick atmospheric bridge, while the delayed response in the subsurface is related to the slow ocean adjustment (e.g., YL05; Wu et al. 2007). In the quasi-equilibrium state, the strength of the Hadley cell, as well as that of the surface trades, are reduced. Furthermore, the anomalous westerly in the tropical Pacific weakens the poleward Ekman transports. The weakened Ekman transport generates anomalous positive convergences of heat transport and makes a major contribution to the maintenance of the tropical Pacific SST warming.

Although our results primarily confirm the main findings of YL05, there are still some differences between our results and YL05. For instance, under similar conditions of prescribed 2°C SST anomalies in the global extratropics, YL05 found that the equatorial Pacific SSTs increased by about 1°C, which is less than the anomaly of 1.5°C presented in our results. Since the surface mixed layer depth in MICOM in the extratropics is deeper than the first level in the MOM results in YL05, the MICOM in this study may favor the release of more heat into the tropics during the process of heat exchanges between the two regions and, hence, strengthen the extratropical impact on the tropics. Differences also appear in the locations of the tropical maximum SST anomalies, that is, in the eastern equatorial Pacific in this study, but in the western Pacific in YL05. The change in zonal heat transport also favors the tropical heat convergence anomaly in this study, which is absent in YL05. All of the differences should be mainly due to the different climate models, particularly the oceanic component in the coupled system.

Besides comparisons with YL05, this study further analyzes the dynamics of the changes of the atmospheric and oceanic circulation patterns. The extratropical influence on the tropical climate variability is achieved by processes in both the atmosphere and the ocean. In the atmosphere, the ITCZ moves southward and eastward, corresponding to a reduction of the Hadley circulation as well as the Walker circulation. In conjunction with the ITCZ displacement, convective precipitation anomalies are formed on the boundary of the climatological ITCZ. The anomalous convections cut off and consume a considerable amount of the water vapor, which suppresses the climatological mean convection in the Southeast Asia region. A similar situation can also be found in the results of global warming experiments (e.g., Fig. 12 in Wetherald and Manabe 2002). Since water vapor plays a key role in the convective activities, the water vapor sources and sinks, as

well as its transport, could help us to draw a clearer picture of the convection changes.

Compared with the quick changes in SSTs, the subsurface temperatures in the tropical Pacific show a large delayed response with time scales of about five decades. Since the STCs reach quasi equilibrium within two decades, the slow response of the subsurface temperature cannot be explained only by the change in strength of the STCs. The delayed evolution of the subsurface temperature in the tropical Pacific can be traced back to the slow changing of the subsurface temperature in the extratropics.

Displayed on time-dependent isopycnal layers, positive subsurface temperature anomalies are present only in the first half of the distance travelled after subduction, and are subsequently replaced by negative temperature anomalies in the deep tropics regions. Observations of the upper-ocean temperature also revealed that temperature anomalies subducted into the pycnocline in the central North Pacific did not reach the equator with any appreciable amplitude, and ceased at approximately 18°N in the western Pacific (Scheider et al. 1999). Since there are no such negative temperature anomalies at these depth levels, the negative temperature anomalies on the time-dependent isopycnals in the tropics may be ascribed to the deepening of the isopycnal layers.

In addition to the isopycnal deepening, the warming and the freshening of the surface mixed layer in the outcropping region can also lead to a cooling (as well as freshening) of the subsurface water on a given isopycnal (Church et al. 1991; Bindoff and McDougall 1994). In the extratropical regions, the surface mixed layer densities become smaller, due to the ocean warming and freshening. As a consequence, outcropping lines of certain isopycnal layers are moved poleward. This process affects the subduction, which can be inferred by the relatively weaker signal of the positive temperature anomalies in the subsurface isopycnal layer in the perturbation experiment. The negative salinity anomalies subducted in the extratropics can counteract apparent positive temperature anomalies by the mechanism of density compensation. The noticeable features of density compensation of temperature and salinity indicate that diapycnal processes play an important role in the equatorward transport of the temperature and salinity anomalies from the midlatitudes.

The differences between our results and YL05 suggest that ensemble experiments, model intercomparison, and more data-based diagnoses are needed in the future to reach more solid conclusions. The strong tropical response to the extratropical warming highlights the role of the extratropics climate change in the tropical climate variability. Therefore, investigations on the tropical climate change should, at the same time, take into account the extratropical climate change.

Acknowledgments. This study has received support from the National Natural Science Foundation of China under Grants 40631005 and 40620130113, the Major Project of Knowledge Innovation Program of the Chinese Academy of Sciences. The model development and integration have been supported by the Research Council of Norway through the RegClim Project and the Supercomputing Programme, and by the European Union DG-XII Climate and Environment Program through DYNAMITE. We thank Ingo Bethke for assistance with the BCM output. Comments from the two anonymous reviewers were helpful to improving the overall quality of the paper.

REFERENCES

Alexander, M. A., I. Bladé, M. Newman, J. R. Lanzante, N. C. Lau, and J. D. Scott, 2002: The atmospheric bridge: The influence of ENSO teleconnections on air–sea interaction over the global oceans. *J. Climate,* **15,** 2205–2231.

Barlow, M., S. Nigam, and E. H. Berbery, 2001: ENSO, Pacific decadal variability, and U.S. summertime precipitation, drought, and stream flow. *J. Climate,* **14,** 2105–2126.

Barnett, D., W. Pierce, M. Latif, D. Dommenget, and R. Saravanan, 1999: Interdecadal interactions between the tropics and midlatitudes in the Pacific basin. *Geophys. Res. Lett.,* **26,** 615–618.

Bentsen, M., H. Drange, T. Furevik, and T. Zhou, 2004: Simulated variability of the Atlantic meridional overturning circulation. *Climate Dyn.,* **14,** doi:10.1007/s00382-004-0397-x.

Bethke, I., T. Furevik, and H. Drange, 2006: Towards a more saline North Atlantic and a fresher Arctic under global warming. *Geophys. Res. Lett.,* **33,** L21712, doi:10.1029/2006GL027264.

Bindoff, N. L., and T. J. McDougall, 1994: Diagnosing climate change and ocean ventilation using hydrographic data. *J. Phys. Oceanogr.,* **24,** 1137–1152.

Bleck, R., C. Rooth, D. Hu, and L. T. Smith, 1992: Salinity-driven thermocline transients in a wind- and thermohaline-forced isopycnic coordinate model of the North Atlantic. *J. Phys. Oceanogr.,* **22,** 1486–1505.

Bonjean, F., and G. S. E. Lagerloef, 2002: Diagnostic model and analysis of the surface currents in the tropical Pacific Ocean. *J. Phys. Oceanogr.,* **32,** 2938–2954.

Capotondi, A., M. A. Alexander, C. Deser, and M. J. McPhaden, 2005: Anatomy and decadal evolution of the Pacific subtropical–tropical cells (STCs). *J. Climate,* **18,** 3739–3758.

Church, J. A., J. S. Godfrey, D. R. Jackett, and T. J. McDougall, 1991: A model of sea level rise caused by ocean thermal expansion. *J. Climate,* **4,** 438–456.

Déqué, M., C. Dreveton, A. Braun, and D. Cariolle, 1994: The ARPEGE/IFS atmosphere model: A contribution to the French community climate modeling. *Climate Dyn.,* **10,** 249–266.

Drange, H., and K. Simonsen, 1996: Formulation of air–sea fluxes in the ESOP2 version of MICOM. Nansen Environmental

and Remote Sensing Center Tech. Rep. 125, Bergen, Norway, 23 pp.

Furevik, T., M. Bentsen, H. Drange, I. K. T. Kindem, N. G. Kvamstø, and A. Sorteberg, 2003: Description and evaluation of the Bergen climate model: ARPEGE coupled with MICOM. *Climate Dyn.,* **21,** 27–51.

Giese, B. S., and J. A. Carton, 1999: Interannual and decadal variability in the tropical and midlatitude Pacific Ocean. *J. Climate,* **12,** 3402–3418.

——, S. C. Urizar, and N. S. Fuckar, 2002: Southern Hemisphere origins of the 1976 climate shift. *Geophys. Res. Lett.,* **29,** 1014, doi:10.1029/2001GL013268.

Graham, N. E., and T. P. Barnett, 1987: Sea surface temperature, surface wind divergence, and convection over the tropical oceans. *Science,* **238,** 657–659.

Gu, D. F., and S. H. Philander, 1997: Interdecadal climate fluctuations that depend on exchanges between the tropics and extratropics. *Science,* **275,** 805–807.

Hoerling, M. P., J. W. Hurrell, and T. Xu, 2001: Tropical origins for recent North Atlantic climate change. *Science,* **292,** 90–92.

Holton, J. R., 2004: *An Introduction to Dynamic Meteorology*. 4th ed. Academic Press, 534 pp.

Kessler, W. S., L. M. Rothstein, and D. Chen, 1998: The annual cycle of SST in the eastern tropical Pacific, diagnosed in an ocean GCM. *J. Climate,* **11,** 777–799.

Kirtman, B. P., and P. S. Schopf, 1998: Decadal variability in ENSO predictability and prediction. *J. Climate,* **11,** 2804–2822.

Kleeman, R., J. P. McCreary, and B. A. Klinger, 1999: A mechanism for generating ENSO decadal variability. *Geophys. Res. Lett.,* **26,** 1743–1746.

Knutson, T. R., and S. Manabe, 1998: Model assessment of decadal variability and trends in the tropical Pacific Ocean. *J. Climate,* **11,** 2273–2296.

Lau, N. C., 1997: Interactions between global SST anomalies and the midlatitude atmospheric circulation. *Bull. Amer. Meteor. Soc.,* **78,** 21–33.

Liu, Z., and H. Yang, 2003: Extratropical control on tropical climate: Atmospheric bridge and oceanic tunnel. *Geophys. Res. Lett.,* **30,** 1230, doi:10.1029/2002GL016492.

——, and M. Alexander, 2007: Atmospheric bridge, oceanic tunnel, and global climatic teleconnections. *Rev. Geophys.,* **45,** RG2005, doi:10.1029/2005RG000172.

——, S. G. H. Philander, and R. C. Paconowski, 1994: A GCM study of tropical–subtropical upper-ocean water exchange. *J. Phys. Oceanogr.,* **24,** 2606–2623.

Lohmann, K., and M. Latif, 2005: Tropical Pacific decadal variability and the subtropical–tropical cells. *J. Climate,* **18,** 5163–5178.

Lu, J., R. J. Greatbatch, and K. A. Peterson, 2004: Trend in Northern Hemisphere winter atmospheric circulation during the last half of the twentieth century. *J. Climate,* **17,** 3745–3760.

McCreary, J. P., and P. Lu, 1994: Interaction between the subtropical and equatorial ocean circulations: The subtropical cell. *J. Phys. Oceanogr.,* **24,** 466–497.

McDougall, T. J., 1987: Neutral surfaces. *J. Phys. Oceanogr.,* **17,** 1950–1964.

McPhaden, M. J., and D. Zhang, 2002: Slowdown of the meridional overturning circulation in the upper Pacific Ocean. *Nature,* **415,** 603–608.

Philander, S. G. H., W. J. Hurlin, and A. D. Seigel, 1987: Simulation of the seasonal cycle of the tropical Pacific Ocean. *J. Phys. Oceanogr.,* **17,** 1986–2002.

Schneider, N., 2000: A decadal spiciness mode in the tropics. *Geophys. Res. Lett.,* **27,** 257–260.

——, A. J. Miller, M. A. Alexander, and C. Deser, 1999: Subduction of decadal North Pacific temperature anomalies: Observations and dynamics. *J. Phys. Oceanogr.,* **29,** 1056–1070.

Schott, F. A., J. P. McCreary, and G. C. Johnson, 2004: Shallow overturning circulations of the tropical–subtropical oceans. *Earth Climate: The Ocean–Atmosphere Interaction, Geophys. Monogr.,* Vol. 147, Amer. Geophys. Union, 261–304.

Sorteberg, A., T. Furevik, H. Drange, and N. G. Kvamstø, 2005: Effects of simulated natural variability on Arctic temperature projections. *Geophys. Res. Lett.,* **32,** L18708, doi:10.1029/2005GL023404.

Timmermann, A., J. Oberhuber, A. Bacher, M. Esch, M. Latif, and E. Roeckner, 1999: Increased El Niño frequency in a climate model forced by future greenhouse warming. *Nature,* **398,** 694–697.

Vimont, D. J., D. S. Battisti, and A. C. Hirst, 2003: The seasonal footprinting mechanism in the CSIRO coupled general circulation models. *J. Climate,* **16,** 2653–2667.

Wang, C., 2002: Atmospheric circulation cells associated with the El Niño–Southern Oscillation. *J. Climate,* **15,** 399–419.

Wetherald, R. T., and S. Manabe, 2002: Simulation of hydrologic changes associated with global warming. *J. Geophys. Res.,* **107,** 4379–4394.

Wong, A., N. Bindoff, and J. Church, 1999: Large-scale freshening of intermediate waters in the Pacific and Indian Oceans. *Nature,* **400,** 440–443.

Wu, L., Z. Liu, R. Gallimore, R. Jacob, D. Lee, and Y. Zhong, 2003: Pacific decadal variability: The tropical Pacific mode and the North Pacific mode. *J. Climate,* **16,** 1101–1120.

——, ——, C. Li, and Y. Sun, 2007: Extratropical control of recent tropical Pacific decadal climate variability: A relay teleconnection. *Climate Dyn.,* **28,** doi:10.1007/s00382-006-0198-5.

Yang, H., and Z. Liu, 2005: Tropical–extratropical climate interaction as revealed in idealized coupled climate model experiments. *Climate Dyn.,* **24,** 863–879.

——, H. Jiang, and B. Tan, 2005: Asymmetric impact of the North and South Pacific on the equator in a coupled climate model. *Geophys. Res. Lett.,* **32,** L05604, doi:10.1029/2004GL021925.

Zhang, Y., and J. M. Wallace, 1996: Is climate variability over the North Pacific a linear response to ENSO? *J. Climate,* **9,** 1468–1478.

Zhou, T. J., R. C. Yu, Y. Q. Gao, and H. Drang, 2006a: Ocean–atmosphere coupled model simulation of North Atlantic interannual variability I: Local air–sea interaction (in Chinese with English abstract). *Acta Meteor. Sin.,* **64,** 1–18.

——, ——, ——, and ——, 2006b: Ocean–atmosphere coupled model simulation of North Atlantic interannual variability II: Tropical tele-connection (in Chinese with English abstract). *Acta Meteor. Sin.,* **64,** 18–30.